Chemical Science

ROYAL SOCIETY OF CHEMISTRY

EDGE ARTICLE

View Article Online
View Journal | View Issue

Cite this: *Chem. Sci.*, 2021, **12**, 3580

All publication charges for this article have been paid for by the Royal Society of Chemistry

Fluorine-induced aggregate-interlocking for color-tunable organic afterglow with a simultaneously improved efficiency and lifetime†

Hui Li,‡[a] Huanhuan Li,‡[a] Jie Gu,[a] Fei He,[a] Hao Peng,[a] Ye Tao,*[a] Dan Tian,[b] Qingqing Yang,[a] Ping Li,[a] Chao Zheng,*[a] Wei Huang [ac] and Runfeng Chen *[a]

Designing organic afterglow materials with a high efficiency and long lifetime is highly attractive but challenging because of the inherent competition between the luminescence efficiency and lifetime. Here, we propose a simple yet efficient strategy, namely fluorine-induced aggregate-interlocking (FIAI), to realize both an enhanced efficiency and elongated lifetime of afterglow materials by stimulating the synergistic effects of the introduced fluorine atoms to efficiently promote intersystem crossing (ISC) and intermolecular non-covalent interactions for facilitating both the generation of triplet excitons and suppression of non-radiative decays. Thus, the fluorine-incorporated afterglow molecules exhibit greatly enhanced ISC with a rate constant up to 5.84×10^7 s^{-1} and suppressed non-radiative decay down to 0.89 s^{-1}, resulting in efficient organic afterglow with a simultaneously improved efficiency up to 10.5% and a lifetime of 1.09 s. Moreover, accompanied by the efficient phosphorescence emission especially at cryogenic temperature, color-tunable afterglow was also observed at different temperatures. Therefore, tri-mode multiplexing encryption devices by combining lifetime, temperature and color, and visual temperature sensing were successfully established. The FIAI strategy by addressing fundamental issues of afterglow emission paves the way to develop high-performance organic afterglow materials, opening up a broad prospect of aggregated and excited state tuning of organic solids for emission lifetime-resolved applications.

Received 2nd November 2020
Accepted 7th January 2021

DOI: 10.1039/d0sc06025a

rsc.li/chemical-science

Introduction

Long afterglow phosphorescent materials, which exhibit persistent luminescence after switching off the irradiation source,[1,2] have recently received exponentially increasing attention, not only because of the significant scientific advance in understanding the rich excited state properties of optoelectronic materials but also owing to the substantial promising applications ranging from emergency display,[3,4] information encryption[5,6] and storage[7] to bio-imaging and therapy.[8–10] Compared to their inorganic afterglow counterparts,[11,12] metal-free organic afterglow materials have many advantages including easy synthesis conditions, low production costs, large molecular versatility, excellent substrate compatibilities, and many others.[2,13,14] However, because of their weak spin–orbit coupling (SOC) with inefficient intersystem crossing (ISC) and severe molecular motion and vibration with rapid non-radiative decays, the design and construction of high-performance organic afterglow materials with a high quantum yield and long lifetime are still very challenging even though they have been achieved in recent years.

Principally, to achieve organic afterglow with a high phosphorescence quantum yield (Φ^{T^*}), it is essential to establish the rapid radiation decay rate ($k_r^{T^*}$), slow non-radiation decay rate ($k_{nr}^{T^*}$) and high ISC efficiency (Φ_{ISC}) for the triplet excited state emission (Fig. 1a, eqn (1) and (2)); nevertheless, fast ($k_r^{T^*}$) implies a short afterglow lifetime (τ^{T^*}), resulting in an inherent interference between Φ^{T^*} and τ^{T^*}. Up to now, most strategies including heavy atom,[15] aromatic carbonyl,[16] and heteroatom incorporation,[17] and host–guest,[18,19] crystallization[20,21] and H-aggregation[8,22] engineering have failed to achieve simultaneously improved Φ^{T^*} and τ^{T^*}. Only limited examples through supramolecular self-assembly,[23] free volume modulation[24] and resonance-activated spin-flipping[25] have shown both improved quantum yields and prolonged lifetimes by breaking through

[a]*Key Laboratory for Organic Electronics and Information Displays & Jiangsu Key Laboratory for Biosensors, Institute of Advanced Materials (IAM), Nanjing University of Posts & Telecommunications, 9 Wenyuan Road, Nanjing 210023, China. E-mail: iamytao@njupt.edu.cn; iamczheng@njupt.edu.cn; iamrfchen@njupt.edu.cn*

[b]*College of Materials Science and Engineering, Nanjing Forestry University, Nanjing 210037, China*

[c]*Frontiers Science Center for Flexible Electronics, Xi'an Institute of Flexible Electronics (IFE) and Xi'an Institute of Biomedical Materials & Engineering, Northwestern Polytechnical University (NPU), 127 West Youyi Road, Xi'an 710072, China*

† Electronic supplementary information (ESI) available. CCDC 149367, 1975648, 1975612, and 1975625. For ESI and crystallographic data in CIF or other electronic format see DOI: 10.1039/d0sc06025a

‡ These authors contributed equally to this work.

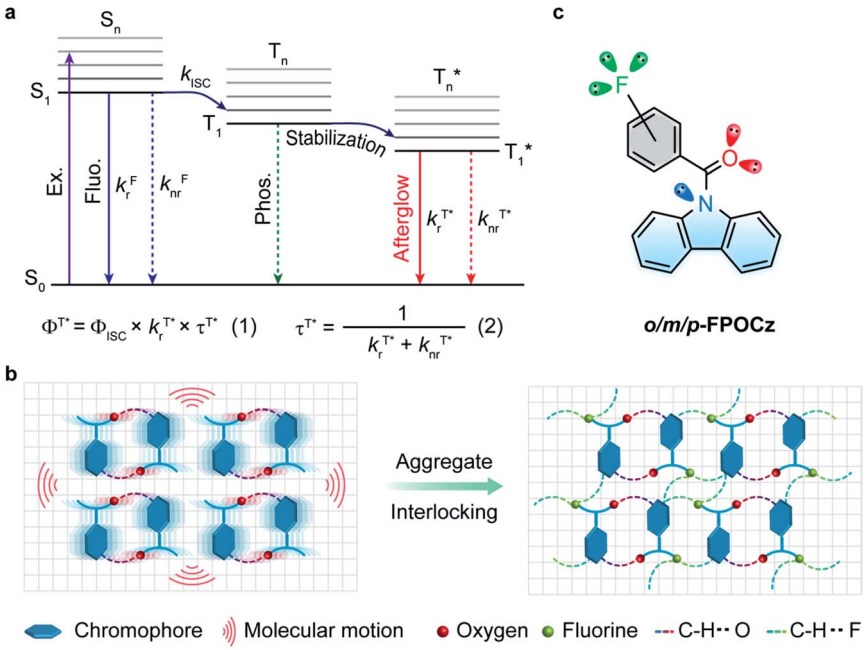

Fig. 1 Design of fluorine-induced aggregate-interlocking (FIAI) for high-performance organic afterglow. (a) Jablonski diagram of the organic afterglow mechanism. The inset shows the equations of the phosphorescence quantum yield (eqn (1)) and lifetime (eqn (2)). (b) Schematic drawing of the FIAI strategy to restrict molecular motions in the crystal. (c) Molecular structures of ***o*/*m*/*p*-FPOCz** designed by FIAI. Ex., excitation; Fluo., fluorescence; Phos., phosphorescence.

the intrinsic bottlenecks of organic afterglow, despite their design and synthetic complications.

Non-covalent interactions that can form an interlocked molecular aggregate have been proved to be effective in suppressing nonradiative decay.[26] Fluorine with a small size and high electronegativity has been known as an influential moiety to construct unique intra- and intermolecular non-covalent interactions in the fields of optoelectronic materials[27] for achieving a dense molecular aggregation network in the solid state,[28] especially in preparing donor and acceptor molecules for organic photovoltaics.[29,30] Inspired by the intensive fluorine-induced non-covalent interactions, we envision that the incorporation of fluorine atoms into molecular crystals would greatly inhibit non-radiative transition. Particularly, the motion of an aggregated dimer in a conventional molecular crystal would induce the strong consumption of triplet excitons under ambient conditions (Fig. 1b, left), leading to relatively poor afterglow properties. After the introduction of fluorine atoms, the adjacent dimers can be effectively interlocked through efficient non-covalent interactions (Fig. 1b, right), leading to the efficient stabilization of triplet excitons for reinforced afterglow performance; meanwhile, the multiple lone-pair electrons of the fluorine atom could potentially favor n–π^* transition to facilitate the ISC process for the population of triplet excitons. With these extraordinary characteristics of the fluorine atom in mind, we propose a new strategy of fluorine-induced aggregate-interlocking (FIAI) to design and prepare three afterglow isomers of ***o*/*m*/*p*-FPOCz** at different fluorine substitution positions to simultaneously improve the lifetime and promote the ISC of organic afterglow (Fig. 1c). Indeed, significantly boosted afterglow performance with enhanced ISC rates (k_{ISC}^{min}s) up to 5.84×10^7 s^{-1} and suppressed $k_{nr\,max}^{T*}$ down to 0.89 s^{-1} for excellent afterglow emission with both an enlarged ultralong lifetime up to 1.09 s and an improved afterglow yield of 10.5% was achieved in the resultant afterglow molecules under ambient conditions, breaking the inherent conflict between the afterglow lifetime and efficiency. More interestingly, these afterglow isomers designed by the FIAI strategy also demonstrate both phosphorescence emission from T_1 and afterglow emission from T_1^* at cryogenic temperature, leading to color-tunable afterglow emission at different temperatures. On account of these distinguished afterglow properties, a tri-mode (lifetime, temperature and color) multiplexing encryption device and temperature sensing chart were realized on flexible substrates for the first time. These findings illustrate a fundamental advancement of purely organic afterglow molecules with the aid of the FIAI tactic in simultaneously elongating the emission lifetime and enhancing the afterglow efficiency, shedding light on the rational molecule design of high-performance organic afterglow materials for advanced lifetime-resolved applications.

Results and discussion

The fluorine-incorporated isomers of ***o*/*m*/*p*-FPOCz** designed by the FIAI strategy were facilely synthesized by a one-step C–N coupling[31] with high yields up to 85% and completely characterized using nuclear magnetic resonance (NMR) spectra, high resolution mass spectra (HRMS), and high-performance liquid chromatogram (HPLC) spectra as well as single crystal and

thermal property analyses (Scheme S1 and Fig. S1–S14†). The recently reported afterglow molecule of (9*H*-carbazol-9-yl)(phenyl) methanone (**POCz**) without fluorine substitution was also prepared for comparative investigation (Scheme S1†).[32]

The photophysical properties of ***o*/*m*/*p*-FPOCz** in dilute tetrahydrofuran solution are almost identical to those of fluorine-free **POCz**, showing absorption peaks at ~279, 305 and 316 nm and steady-state photoluminescence (SSPL) bands at ~338 and 354 nm with nanosecond lifetimes (Fig. S15 and S16†) at room temperature. The low temperature SSPL spectra of ***o*/*m*/*p*-FPOCz** and **POCz** exhibit not only fluorescence bands at ~338 and 354 nm but also obvious phosphorescence emission bands peaking at ~415 and 445 nm with lifetimes up to several seconds because of the suppressed nonradiative transition processes at 77 K (Fig. S17–S19†); notably, the phosphorescence intensities of ***o*/*m*/*p*-FPOCz** are even stronger than those of their corresponding fluorescence bands, while the fluorescence intensity of **POCz** is higher than phosphorescence intensity (Fig. S17†). The large difference between the fluorescence spectra of ***o*/*m*/*p*-FPOCz** and **POCz** at 77 K in solution should be due to the combined results of the fluorine promoted ISC for the enhanced population of triplet excitons and low-temperature suppressed non-radiative transitions for achieving enhanced phosphorescence emission of ***o*/*m*/*p*-FPOCz**. Strikingly, as shown in Fig. 2a, the crystals of the four molecules show intense blue short-lived fluorescence bands with nanosecond lifetimes (Fig. S20†) and efficient yellow afterglow emission with an ultralong lifetime up to several seconds at room temperature (Fig. 2b and c). ***o*/*m*/*p*-FPOCz** reveal a shorter fluorescence lifetime than **POCz** (Fig. S20†), confirming again the promoted ISC process induced by fluorine incorporation. These afterglow molecules demonstrate quite similar afterglow spectra profiles, showing unchanged main afterglow emission peaks at ~527 nm when tuning the excitation light from 300 to 400 nm (Fig. 2d and S21–S24†), the irradiation excitation power from 0.11 to 1.33 mW cm^{-2} (Fig. S25†) and the irradiation time from 0.01 to 10 s, respectively (Fig. S26†). The τ^{T^*} and Φ^{T^*} of **POCz** are 0.75 s and 1.6%. These data are slightly different from the previous results,[31,32] which may be due to the different aggregation states of the crystals. Importantly, the afterglow performance of the ***o*/*m*/*p*-FPOCz** crystals is much better than that of **POCz**; τ^{T^*}/Φ^{T^*} increases from 0.75 s/1.6% for **POCz** to 0.83 s/2.6%, 0.98 s/10.5% and 1.09 s/3.4% for ***o*-FPOCz**, ***m*-FPOCz** and ***p*-FPOCz**, respectively (Fig. 2c and Table S1†), clearly illustrating simultaneous increments in both afterglow lifetime and efficiency.

To quantify the enhancement effects of the FIAI strategy on afterglow performance, the rate constant analyses of k_{ISC}, $k_r^{T^*}$ and $k_{nr}^{T^*}$ of ***o*/*m*/*p*-FPOCz** and **POCz** were performed. As shown in Fig. 2c, the k_{ISC}^{min} of ***o*-FPOCz**, ***m*-FPOCz** and ***p*-FPOCz** crystals reached 9.70×10^6, 5.84×10^7 and 1.73×10^7 s^{-1} respectively, which are about 7-, 54- and 13-folds larger than that of **POCz** (1.32×10^6 s^{-1}), confirming experimentally the enhanced ISC for increasing the afterglow efficiency; meanwhile, the $k_{nr\,max}^{T^*}$, which plays a key role in manipulating the phosphorescence lifetime, of ***o*-FPOCz**, ***m*-FPOCz** and ***p*-FPOCz** crystals also decreases to 1.17, 0.93 and 0.89 s^{-1}, which are 0.89-, 0.71- and 0.68-folds that of POCz (1.31 s^{-1}), respectively; and ***o*/*m*/*p*-FPOCz** crystals also exhibit higher $k_r^{T^*}$ than **POCz** (Table S1†). The enhanced k_{ISC}, and $k_r^{T^*}$, and decreased $k_{nr}^{T^*}$ of ***o*/*m*/*p*-FPOCz**

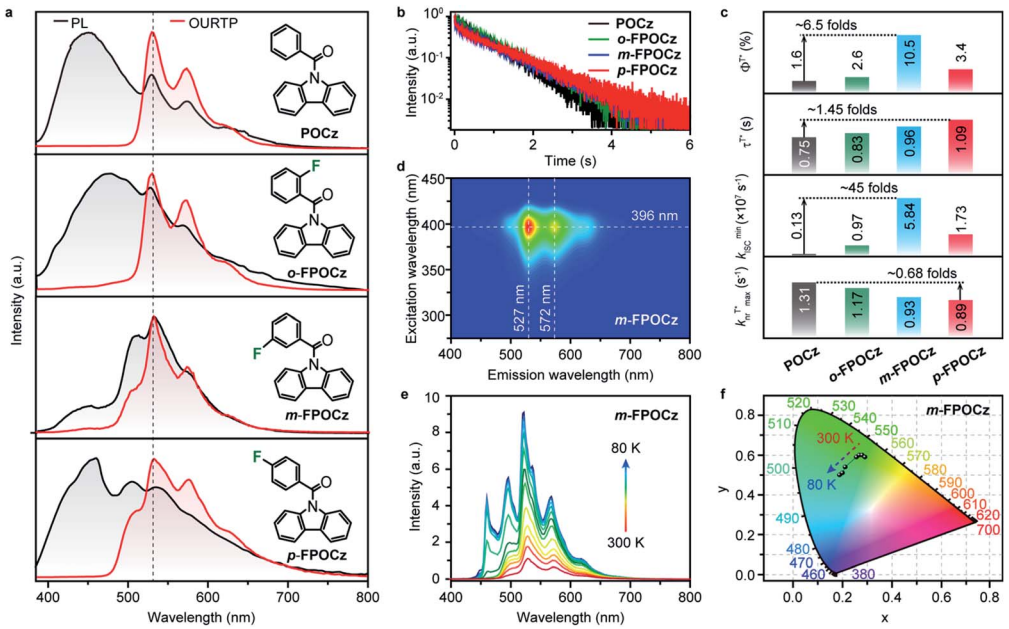

Fig. 2 Photophysical properties of **POCz** and ***o*/*m*/*p*-FPOCz**. (a) Steady-state photoluminescence (black lines) and afterglow spectra (red lines) under ambient conditions. Insets show the molecular structures. (b) Afterglow decay profiles of the emission bands at 527 nm by 365 nm excitation under ambient conditions. (c) Key parameters for organic afterglow emission. (d) Excitation-phosphorescence mapping of the ***m*-FPOCz** crystal with a delay time of 25 ms. (e) Temperature-dependent afterglow spectra from 300 to 80 K of the ***m*-FPOCz** crystal. (f) CIE 1931 coordinates of afterglow emission of the ***m*-FPOCz** crystal from 300 to 80 K.

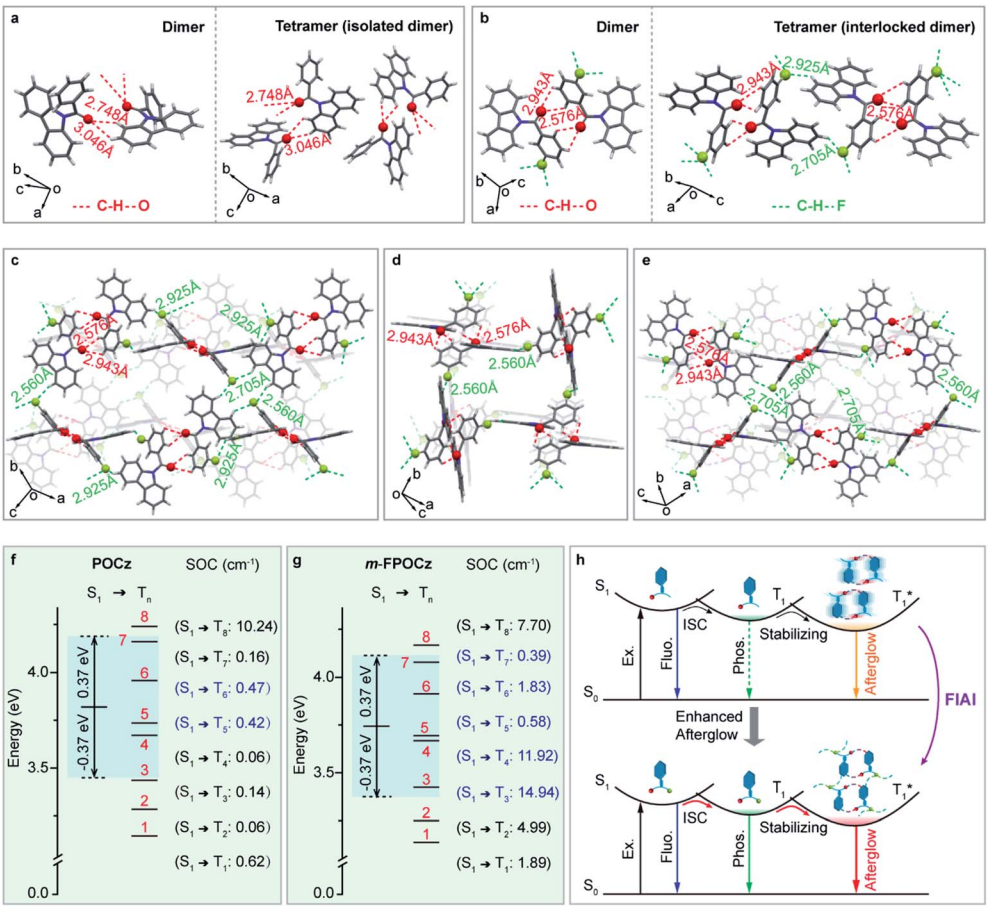

Fig. 3 Single crystal and theoretical analyses. (a and b) Intermolecular interactions of the selected dimer (left) and tetramer (right) in **POCz** (a) and *m*-FPOCz (b) single crystals. (c–e) The molecular packing arrangements along different directions in the *m*-FPOCz single crystal showing various intermolecular interactions. (f and g) TD-DFT calculated energy level diagram and the corresponding SOC constants of **POCz** (f) and *m*-FPOCz (g). (h) Proposed mechanism in boosting the organic afterglow performance *via* FIAI.

should be responsible for the simultaneously elongated lifetime and high efficiency,[33] verifying the significant role of fluorine-substitution in boosting afterglow performance.

We further explore the influence of temperature and atmosphere on the unique afterglow emission. On decreasing from 300 to 80 K, the intensity of the afterglow emission of **POCz** and ***o*/*m*/*p*-FPOCz** at 527 nm from T_1^* increases; interestingly, in comparison to **POCz**, a new emission band centered at about 460 nm appears in ***o*/*m*/*p*-FPOCz** crystals and the corresponding intensities also increase when the temperature decreases; and because of different increases in phosphorescent intensity at 527 nm and 460 nm, color-tunable afterglow emissions at different temperatures in ***o*/*m*/*p*-FPOCz** crystals were achieved (Fig. 2e and f and S27–S30†). To figure out the origin of the new emission band, the phosphorescence spectra of ***m*-FPOCz**, as a model molecule, at 80 K were recorded. As shown in Fig. S31,† ***m*-FPOCz** reveals a main emission band around 460 nm in both pure and doped films, suggesting that the emission band at ~460 nm in ***o*/*m*/*p*-FPOCz** crystals should be attributed to the radiative decay from T_1 of the amorphous state. The crystals of ***o*/*m*/*p*-FPOCz** show almost identical afterglow spectra and lifetime decay profiles in air, argon (Ar) and oxygen (O_2). In contrast, the afterglow emission and lifetime of **POCz** were slightly enhanced in Ar and decreased in O_2 compared to those in an air atmosphere (Fig. S32–S36†).

To exactly understand the improved afterglow performance of fluorine-substituted afterglow molecules, we further analyzed the molecular packing modes and intermolecular interactions in single crystals. As shown in Fig. 3a (left), obvious intermolecular interactions of C–H···O with distances of 3.046 and 2.748 Å were observed in the dimer of the **POCz** crystal. Nevertheless, because there are no intermolecular interactions between adjacent dimers (Fig. 3a, right and S37†), the facile molecular motion and vibration induce severe non-radiative decays (Fig. 1b, left), thereby leading to relatively poor afterglow performance of **POCz**. In contrast, besides various C–H···O interactions in the dimers of the ***o*/*m*/*p*-FPOCz** crystals (Fig. 3b, left and S38a and S39a†), there are also abundant intermolecular interactions of C–H···F in the neighboring dimers for further suppressed non-radiative decays (Fig. 3c–e, S38b, c and S39b, c†). The enhanced intermolecular interactions of ***o*/*m*/*p*-FPOCz** compared to **POCz** can be experimentally verified by more stable afterglow emission and lifetimes in different atmospheres of Ar, air and O_2 (Fig. S32–S36†) and theoretically

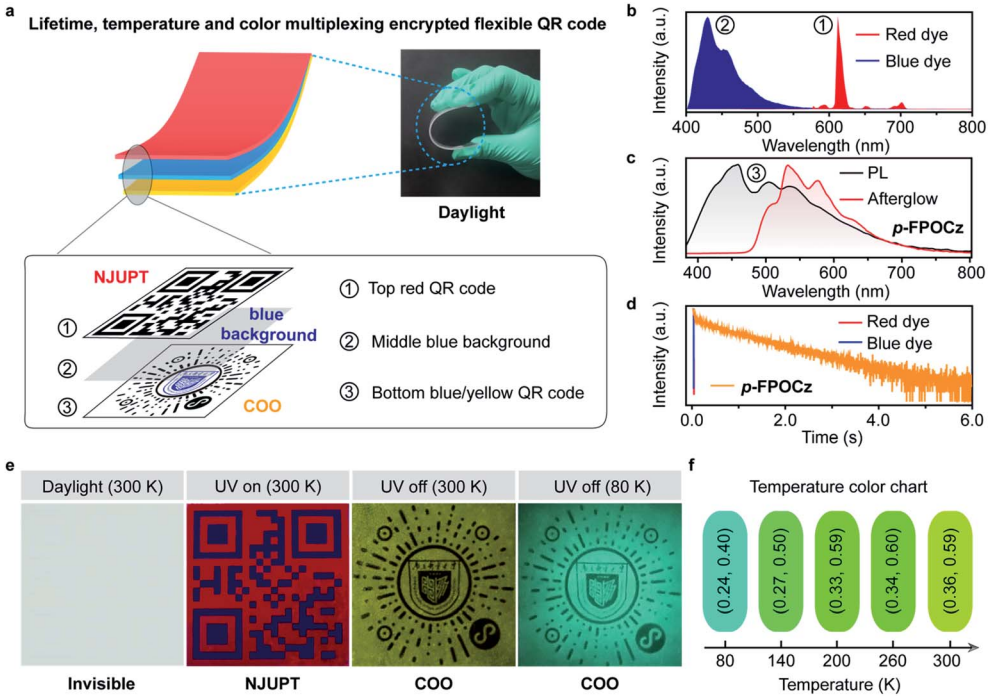

Fig. 4 Applications of the afterglow materials designed by the FIAI strategy. (a). Schematic construction of the lifetime, temperature and color tri-mode multiplexing encryption QR code. (b) Fluorescence spectra of red and blue dyes. (c) Steady-state (black) and afterglow emission spectra (red) of the ***p*-FPOCz** crystal. (d) Lifetime decay profiles of the short-lived luminescence of the red and blue dyes and the ***p*-FPOCz** crystal. (e) Photographs of the lifetime, temperature and color multiplexing encryption QR code under daylight and 365 nm irradiation and after ceasing the irradiation. (f) Temperature-dependent color chart with the corresponding CIE coordinate manifesting the feasibility of the ***p*-FPOCz** crystal in visual detection of temperature.

revealed by independent gradient model (IGM) analysis showing a larger IGM isosurface with stronger interactions between neighboring molecules (Fig. S40†). Meanwhile, powder XRD measurements were also performed to further verify the enhanced intermolecular interactions in the ***o*/*m*/*p*-FPOCz** crystals. An obvious difference could be visually observed in their XRD spectra (Fig. S41†), showing much more sharp peaks ranging from 20 to 50° in the curve of ***o*/*m*/*p*-FPOCz**, which indicate their enhanced interactions and rigidities compared to **POCz**. Additionally, multiple H-aggregations that are very crucial in achieving efficient afterglow emission were found in the ***o*/*m*/*p*-FPOCz** single crystals (Table S3†). These strong intermolecular interactions can effectively facilitate the formation of steric-interlocked molecular aggregates along different directions in single crystals to greatly inhibit non-radiative decays, leading to high afterglow performance.

To theoretically investigate the promoted ISC through fluorine incorporation, time dependent density functional theory (TD-DFT) and Dalton calculations were carried out.[34,35] From the simulated excited state energy levels, there are multiple triplet states in ***o*/*m*/*p*-FPOCz** molecules with the singlet and triplet splitting energy (ΔE_{ST}) lower than 0.37 eV for achieving possible ISC channels according to the energy gap law.[36] Moreover, the feasible ISC process can be further confirmed by large SOC values according to the EI-sayed rule.[37] Indeed, the SOC values of ***o*/*m*/*p*-FPOCz** are greatly larger than that of **POCz** (Fig. 3f and g and S42†). On the basis of small ΔE_{ST} (<0.37 eV) and large SOC values (>0.3 cm^{-1}), the number of efficient ISC channels predicted in **POCz**, ***o*-FPOCz**, ***m*-FPOCz** and ***p*-FPOCz** is 2, 3, 5 and 4, clearly indicating the enhanced ISC process in fluorine-substituted isomers;[38] moreover, the larger SOC values and stronger intermolecular interactions in ***m*-FPOCz** crystals should be the main reason for their higher afterglow efficiency. On account of both experimental and theoretical investigations, the facilitated organic afterglow of the fluorine-incorporated molecules could be ascribed to suppressed non-radiative transition and promoted ISC achieved by the FIAI strategy (Fig. 3h).

Given the extraordinary ultralong-lived and temperature-dependent color-tunable feature of the afterglow molecules designed *via* the FIAI strategy, we take one step further to demonstrate the potential applications of these promising afterglow materials in the fields of lifetime, temperature and color tri-mode multiplexing encryption quick response (QR) code as well as visual sensing of cryogenic temperature (Fig. 4 and S43†). The multilayer QR code comprises a top short-lived fluorescence red and blue QR layer (NJUPT) and a bottom ultralong lived yellow afterglow QR (COO) layer (Fig. 4a–d). As shown in Fig. 4e, the multilayer QR code is very difficult to observe in daylight. Under irradiation using a 365 nm UV-lamp, the top red and blue QR layer can be facilely captured and identified using a commercial mobile-phone displaying the information of "NJUPT" and the bottom QR layer showing blue emission under 365 nm irradiation is actually indiscernible because of the interference of the middle blue fluorescence

background layer. After the ceasing of 365 nm irradiation light, the short-lived background fluorescence interference immediately vanishes; the bottom yellow afterglow QR code layer appears and can be seen showing the varied information of "COO" (Fig. 4e). And, on cooling from room temperature to 80 K, the emission color of the bottom afterglow QR code layer changes from yellow to blue-green, demonstrating its unique feature of lifetime, temperature and color-based tri-mode encryption, and visual multicolor display for quantitative temperature sensing (Fig. 4f).

Conclusions

In summary, we propose a new strategy to simultaneously enhance the efficiency and lifetime of organic afterglow materials by fluorine-induced molecular aggregate interlocking. The introduction of fluorine atoms can not only favor n–π* transition to promote the ISC process, but can also form strong noncovalent intermolecular interactions between adjacent molecules to suppress the molecular vibration and motion of dimers. Consequently, **o/*m*/*p*-FPOCz** demonstrate greatly elevated ISC rates up to 5.84×10^7 s^{-1} and remarkably suppressed $k_{nr}^{T^*}$ down to 0.89 s^{-1}, thus resulting in significantly boosted afterglow emission with a lifetime up to 1.09 s and efficiency of 10.5% under ambient conditions. More impressively, with dual phosphorescence from amorphous T_1 and aggregated T_1^* at cryogenic temperature, color-tunable afterglow emission at different temperatures was achieved. Thus, the tri-mode multiplexing encryption QR code and temperature sensing were successfully established based on the prominent high-efficiency, ultralong-lifetime and color-tunable nature of the organic afterglow molecules designed by the FIAI strategy. These results of simultaneously achieving the afterglow lifetime and efficiency *via* FIAI furnish a simple but efficient approach in developing high-performance organic afterglow molecules, providing an exciting and promising avenue to overcome the intrinsic conflict between the afterglow efficiency and lifetime for fascinating applications.

Conflicts of interest

There are no conflicts to declare.

Acknowledgements

This study was supported in part by the National Natural Science Foundation of China (21704042, 62075102, 21604039, 61875090, 91833306, 22075149 and 21674049), the Six Talent Plan of Jiangsu Province (XCL-049), 1311 Talents Program of Nanjing University of Posts and Telecommunications (Dingshan), Natural Science Fund for Colleges and Universities in Jiangsu Province (Grant No. 17KJB150017), China Postdoctoral Science Foundation funded project (2018M642284), Nanjing University of Posts and Telecommunications Start-up Fund (NUPTSF) (NY219007 and NY217140), and Postgraduate Research & Practice Innovation Program of Jiangsu Province (46030CX18011).

Notes and references

1 Kenry, C. Chen and B. Liu, *Nat. Commun.*, 2019, **10**, 2111.
2 S. Xu, R. Chen, C. Zheng and W. Huang, *Adv. Mater.*, 2016, **28**, 9920.
3 L. Gu, H. Shi, L. Bian, M. Gu, K. Ling, X. Wang, H. Ma, S. Cai, W. Ning, L. Fu, H. Wang, S. Wang, Y. Gao, W. Yao, F. Huo, Y. Tao, Z. An, X. Liu and W. Huang, *Nat. Photonics*, 2019, **13**, 406.
4 W. Li, Q. Huang, Z. Mao, J. Zhao, H. Wu, J. Chen, Z. Yang, Y. Li, Z. Yang, Y. Zhang, M. P. Aldred and Z. Chi, *Angew. Chem., Int. Ed.*, 2020, **59**, 3739.
5 H. Li, H. Li, W. Wang, Y. Tao, S. Wang, Q. Yang, Y. Jiang, C. Zheng, W. Huang and R. Chen, *Angew. Chem., Int. Ed.*, 2020, **59**, 4756.
6 Y. Su, S. Z. F. Phua, Y. Li, X. Zhou, D. Jana, G. Liu, W. Q. Lim, W. K. Ong, C. Yang and Y. Zhao, *Sci. Adv.*, 2018, **4**, eaas9732.
7 M. Gmelch, H. Thomas, F. Fries and S. Reineke, *Sci. Adv.*, 2019, **5**, u7310.
8 J. Jin, H. Jiang, Q. Yang, L. Tang, Y. Tao, Y. Li, R. Chen, C. Zheng, Q. Fan, K. Y. Zhang, Q. Zhao and W. Huang, *Nat. Commun.*, 2020, 11.
9 J. Yang, X. Zhen, B. Wang, X. Gao, Z. Ren, J. Wang, Y. Xie, J. Li, Q. Peng, K. Pu and Z. Li, *Nat. Commun.*, 2018, **9**, 840.
10 X. Chen, C. Xu, T. Wang, C. Zhou, J. Du, Z. Wang, H. Xu, T. Xie, G. Bi, J. Jiang, X. Zhang, J. N. Demas, C. O. Trindle, Y. Luo and G. Zhang, *Angew. Chem., Int. Ed.*, 2016, **55**, 9872.
11 R. Hu, Y. Zhang, Y. Zhao, X. Wang, G. Li and C. Wang, *Chem. Eng. J.*, 2020, **392**, 124807.
12 K. Van den Eeckhout, D. Poelman and P. Smet, *Materials*, 2013, **6**, 2789.
13 L. Huang, B. Chen, X. Zhang, C. O. Trindle, F. Liao, Y. Wang, H. Miao, Y. Luo and G. Zhang, *Angew. Chem., Int. Ed.*, 2018, **57**, 16046.
14 S. Zheng, T. Zhu, Y. Wang, T. Yang and W. Z. Yuan, *Angew. Chem., Int. Ed.*, 2020, **59**, 10018.
15 P. Xue, P. Wang, P. Chen, B. Yao, P. Gong, J. Sun, Z. Zhang and R. Lu, *Chem. Sci.*, 2017, **8**, 6060.
16 W. Zhao, Z. He, J. W. Y. Lam, Q. Peng, H. Ma, Z. Shuai, G. Bai, J. Hao and B. Z. Tang, *Chem*, 2016, **1**, 592.
17 H. Feng, J. Zeng, P. Yin, X. Wang, Q. Peng, Z. Zhao, J. W. Y. Lam and B. Z. Tang, *Nat. Commun.*, 2020, **11**, 2617.
18 Z. Lin, R. Kabe, K. Wang and C. Adachi, *Nat. Commun.*, 2020, **11**, 191.
19 X. Zhang, L. Du, W. Zhao, Z. Zhao, Y. Xiong, X. He, P. F. Gao, P. Alam, C. Wang, Z. Li, J. Leng, J. Liu, C. Zhou, J. W. Y. Lam, D. L. Phillips, G. Zhang and B. Z. Tang, *Nat. Commun.*, 2019, **10**, 5161.
20 Y. Gong, L. Zhao, Q. Peng, D. Fan, W. Z. Yuan, Y. Zhang and B. Z. Tang, *Chem. Sci.*, 2015, **6**, 4438.
21 W. Zhao, T. S. Cheung, N. Jiang, W. Huang, J. W. Y. Lam, X. Zhang, Z. He and B. Z. Tang, *Nat. Commun.*, 2019, **10**, 1595.
22 Z. An, C. Zheng, Y. Tao, R. Chen, H. Shi, T. Chen, Z. Wang, H. Li, R. Deng, X. Liu and W. Huang, *Nat. Mater.*, 2015, **14**, 685.

23 L. Bian, H. Shi, X. Wang, K. Ling, H. Ma, M. Li, Z. Cheng, C. Ma, S. Cai, Q. Wu, N. Gan, X. Xu, Z. An and W. Huang, *J. Am. Chem. Soc.*, 2018, **140**, 10734.
24 Z. Mao, Z. Yang, Z. Fan, E. Ubba, W. Li, Y. Li, J. Zhao, Z. Yang, M. P. Aldred and Z. Chi, *Chem. Sci.*, 2019, **10**, 179.
25 Y. Tao, R. Chen, H. Li, J. Yuan, Y. Wan, H. Jiang, C. Chen, Y. Si, C. Zheng, B. Yang, G. Xing and W. Huang, *Adv. Mater.*, 2018, **30**, 1803856.
26 H. Ma, H. Yu, Q. Peng, Z. An, D. Wang and Z. Shuai, *J. Phys. Chem. Lett.*, 2019, **10**, 6948.
27 A. A. Berger, J. Völler, N. Budisa and B. Koksch, *Acc. Chem. Res.*, 2017, **50**, 2093.
28 K. Reichenbächer, H. I. Süss and J. Hulliger, *Chem. Soc. Rev.*, 2005, **34**, 22.
29 Y. Li, J. Wang, Y. Liu, M. Qiu, S. Wen, X. Bao, N. Wang, M. Sun and R. Yang, *ACS Appl. Mater. Interfaces*, 2016, **8**, 26152.
30 N. Bauer, Q. Zhang, J. J. Rech, S. Dai, Z. Peng, H. Ade, J. Wang, X. Zhan and W. You, *Nano Res.*, 2019, **12**, 2400.
31 Y. Xie, Y. Ge, Q. Peng, C. Li, Q. Li and Z. Li, *Adv. Mater.*, 2017, **29**, 1606829.
32 S. Cai, H. Shi, J. Li, L. Gu, Y. Ni, Z. Cheng, S. Wang, W. Xiong, L. Li, Z. An and W. Huang, *Adv. Mater.*, 2017, **29**, 1701244.
33 S. Hirata, *Adv. Opt. Mater.*, 2017, **5**, 1700116.
34 J. Yuan, R. Chen, X. Tang, Y. Tao, S. Xu, L. Jin, C. Chen, X. Zhou, C. Zheng and W. Huang, *Chem. Sci.*, 2019, **10**, 5031.
35 J. Yuan, S. Wang, Y. Ji, R. Chen, Q. Zhu, Y. Wang, C. Zheng, Y. Tao, Q. Fan and W. Huang, *Mater. Horiz.*, 2019, **6**, 1259.
36 T. Chen, L. Zheng, J. Yuan, Z. An, R. Chen, Y. Tao, H. Li, X. Xie and W. Huang, *Sci. Rep.*, 2015, **5**, 10923.
37 J. Zhao, W. Wu, J. Sun and S. Guo, *Chem. Soc. Rev.*, 2013, **42**, 5323.
38 Y. Tao, K. Yuan, T. Chen, P. Xu, H. Li, R. Chen, C. Zheng, L. Zhang and W. Huang, *Adv. Mater.*, 2014, **26**, 7931.